CHEMISTRY OF MATERIALS

Article

pubs.acs.org/cm

Multicomponent Metal–Organic Frameworks as Defect-Tolerant Materials

Seok J. Lee,[†] Celine Doussot,[†] Anthony Baux,[†] Lujia Liu,[†] Geoffrey B. Jameson,[†] Christopher Richardson,[‡] Joshua J. Pak,[§] Fabien Trousselet,[∥] François-Xavier Coudert,[∥] and Shane G. Telfer*[,†]

[†]MacDiarmid Institute for Advanced Materials and Nanotechnology, Institute of Fundamental Sciences, Massey University, Palmerston North 5301, New Zealand

[‡]School of Chemistry, University of Wollongong, Wollongong, New South Wales 2522, Australia

[§]Department of Chemistry, Idaho State University, Pocatello, Idaho 83201, United States

[∥]PSL Research University, Chimie ParisTech, CNRS, Institut de Recherche de Chimie Paris, 75005 Paris, France

Supporting Information

ABSTRACT: Multicomponent metal–organic frameworks (MOFs) comprise multiple, structurally diverse linkers fixed into an ordered lattice by metal ions or clusters as secondary building units (SBUs). Here, we show how multicomponent MOFs are ideal platforms for engineering materials with high levels of vacancy defects. First, a new type of quaternary MOF that is built up from two neutral, linear ditopic linkers, a 3-fold-symmetric carboxylate ligand, and a dinuclear paddlewheel SBU was synthesized. This MOF, named MUF-32 (MUF = Massey University Framework), is constructed from dabco, 4,4′-bipyridyl (bipy), 4,4′,4″-nitrilotrisbenzoate (ntb), and zinc(II), and it adopts an **ith-d** topology. The zinc(II) ions and ntb ligand define an underlying $[Zn_2(ntb)_{4/3}]$ sublattice (with **pto** topology) that is "load bearing" and maintains the structural integrity of the framework. On the other hand, the dabco and bipy ligands are "decorative", and high levels of vacancy defects can be introduced by their partial omission or removal. These defects can be generated by direct synthesis or by postsynthetic modification. The framework structure, crystallinity, and porosity are maintained even when vacancy levels of 80% are reached. Defect healing is possible by introducing free ligands in a solvent-assisted process to restore pristine MUF-32. Computational analysis reveals that the mechanical instability of the $[Zn_2(ntb)_{4/3}]$ sublattice sets an upper limit on defect levels in this material.

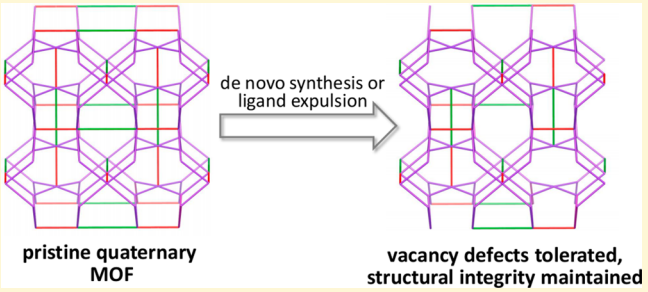

INTRODUCTION

Building metal–organic frameworks (MOFs) from multiple organic linkers has emerged as a fruitful strategy for obtaining materials with remarkable properties.[1,2] There are two categories of such MOFs: (1) *multivariate MOFs* in which the linkers have identical backbones and (2) *multicomponent MOFs* in which the linkers are structurally distinct. While exceptional functional behavior has been observed for some MOFs in category 1,[3,4] the linkers are imperfectly ordered, which leads to pore heterogeneity. We[5,6] and others[2,7−15] have focused on frameworks in the second category. Since the ligands are distinct, they can be discriminated during crystallization of the MOF and occupy specific positions in the lattice. For example, UMCM-1 comprises btb (benzene-1,3,5-tribenzoate) and bdc (benzene-1,4-dicarboxylate) linkers riveted in place by Zn_4O secondary building units (SBUs).[16] The MUF-7 and MUF-77 families are quaternary MOFs constructed from Zn_4O clusters, bdc, bpdc (biphenyl-4,4′-dicarboxylate), and 3-fold symmetric carboxylate ligands.[5,6] Here, the distinct lengths of the bdc and bpdc linkers allow them to be differentiated during framework assembly and located in specific lattice positions. Owing to their structural regularity, insights into the relationship between ligand structure, pore topography, and guest uptake can be drawn from these multicomponent MOFs.

A number of MOFs with defects has emerged in the recent literature, and beneficial impacts of defects on framework properties have been established.[17] Notable examples include the report from Li et al. on the creation of ordered vacancies in a cubic MOF based on Zn(II) and pyrazole-carboxylic acid by removing a quarter of the metal ions and half of the linkers.[18] This provides access to a host of materials with intricate, ordered structures that cannot be synthesized directly. Partial replacement of the terephthalate linkers by capping trifluoroacetate ligands introduces large pores and open metal sites in UiO-66, which render this MOF catalytically active for Meerwein reduction reactions.[19] Advances in the character-

Received: November 8, 2015
Revised: December 4, 2015
Published: December 21, 2015

DOI: 10.1021/acs.chemmater.5b04306
Chem. Mater. 2016, 28, 368−375

ization of defective frameworks have also propelled our understanding of the distribution and properties of defects in MOF crystals.[20,21]

We propose that multicomponent MOFs can serve as platforms for generating materials with high levels of vacancy defects. This concept has parallels with architectural principles where buildings are designed with both "load-bearing" and "decorative" walls. Our strategy, as detailed herein, involves the design of multicomponent MOFs in which certain components are essential for maintaining structural integrity (load-bearing), while other components are nonessential (decorative). Since the absence of these decorative components can be tolerated by the framework, vacancy defects are easily generated.

MOFs with an **ith-d** topology are well-suited to this strategy. Such frameworks can be deconstructed into two subcomponents: an underlying **pto** sublattice (Figure 1a) and linear struts

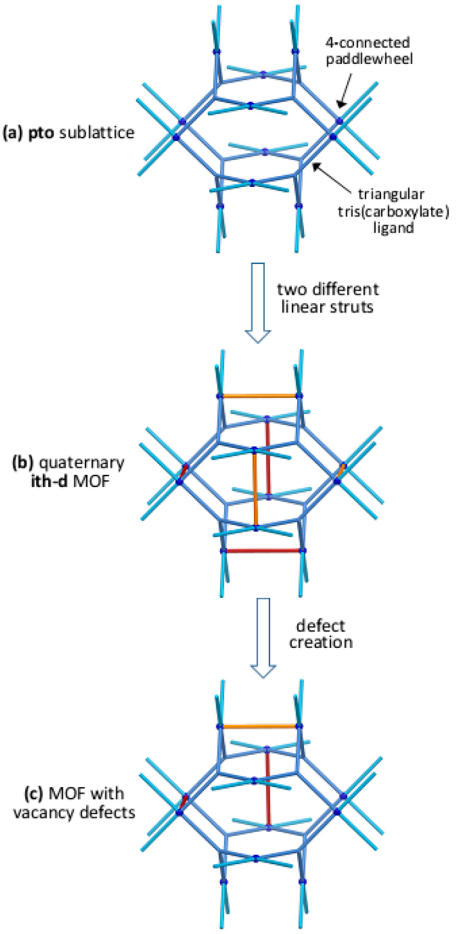

Figure 1. (a) A load-bearing sublattice with a **pto** topology is readily constructed from triangular tris(carboxylate) ligands and metal paddlewheel SBUs. (b) Adding two different linear struts to the **pto** lattice generates a quaternary MOF with an **ith-d** topology. (c) Since the linear struts are not essential to the structural integrity of the MOF, vacancy defects can be sustained.

(Figure 1b).[22,23] These struts link adjacent square planar four-connected nodes of the **pto** net to produce the **ith-d** net.[24] Translating this to feasible chemical building blocks, $[M_2(L)_{4/3}]$ nets with the **pto** topology are readily generated by combining triangular tris(carboxylate) ligands and paddlewheel metal nodes into lattices.[25−31] For the linear struts there are several requirements: (i) they must coordinate via one donor atom to the axial sites of the paddlewheel nodes, (ii) they must be neutral so that charge balance is maintained in their absence, and (iii) they must be of a suitable length to bridge the gap between adjacent nodes.

On the basis of the foregoing considerations we identified dabco and bipy (4,4′-bipyridine) as potentially useful linear struts. With respect to point (iii) above, the two ligands have an average length of 9.0 Å (Table 1). When combined with ntb,

Table 1. Ligand Length Ratios, Given by the Formula [Twofold Linker Length]/[Threefold Linker Length], for Ligand Sets of Known and Putative Ternary and Quaternary Metal−Organic Frameworks[I]

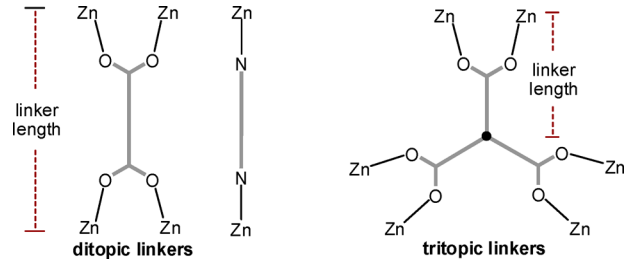

		tritopic	
		ntb	btb
ditopic	length[a]	8.1	9.6
dabco	6.7	0.83[c]	0.70
bipy	11.3	1.40[c]	**1.18**[e]
dabco/bipy	9.0[b]	**1.11**[c]	0.94
bdc	10.1	1.25[d]	1.05[f]
ndc	12.8	1.58	**1.33**[g]
bpdc	14.9	1.84	1.55
bdc/bpdc	12.5[b]	1.54	**1.30**[h]

[a]In Å. [b]Average length of ligand pair. [c]This work. [d]UMCM-4.[9] [e]FJI-1/DUT-23.[22,23] [f]UMCM-1.[16] [g]MOF-205/DUT-6.[14,32] [h]MUF-7.[5] ntb = 4,4′,4″-nitrilotrisbenzoate. [I]The length ratios of known frameworks with an **ith-d** topology are bolded.

the length ratios given by the equation [2-fold linker length]/[3-fold linker length] is 1.11. This is close to the ratio of 1.18 found in $[Zn_2(btb)_{4/3}(bipy)]$,[22,23] which implies that a linker set of ntb, bipy, and dabco is geometrically compatible for coassembly into a quaternary MOF. The utility of linker length ratios in formulating viable multicomponent MOF ligand sets is highlighted in Table 1 by the examples of $[Zn_4O(btb)_{4/3}(ndc)]$[14,32] (ndc = naphthalene-2,6-dicarboxylate) and MUF-7. Since their linker length ratios are very similar (1.33 and 1.30, respectively), in conjunction with Zn_4O nodes both btb/ndc and btb/bpdc/bdc linker sets readily assembly into MOFs with the same **ith-d** topology.

We herein report the successful demonstration that multicomponent MOFs are excellent platforms for creating materials with vacancy defects. We show how Zn(II) paddlewheel nodes and ntb linkers combine to generate a load-bearing **pto** sublattice, which can be cross-linked into an **ith-d** net by bipy and dabco ligands. Since these latter linkers are not required for structural integrity, high levels of vacancy defects can be tolerated (Figure 1c).

RESULTS AND DISCUSSION

Synthesis of MUF-32. We were delighted to find that the reaction of H_3ntb, bipy, and dabco (Figure 2) with $Zn(NO_3)_2$

DOI: 10.1021/acs.chemmater.5b04306
Chem. Mater. 2016, 28, 368−375

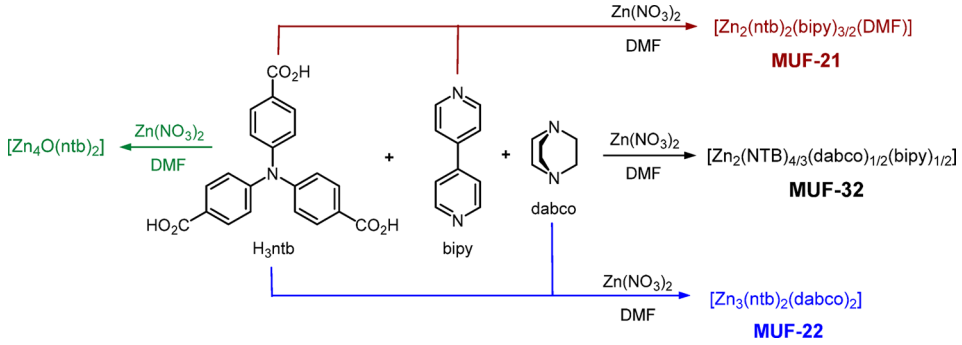

Figure 2. Quaternary metal−organic framework MUF-32 is formed from a three-membered ligand set (ntb, bipy, and dabco) in combination with zinc(II) ions. Two ternary MOFs, MUF-21 and MUF-22, are also reported here. $[Zn_4O(ntb)_2]$ is a known compound.[33]

in DMF produces a framework with the formula $[Zn_2(ntb)_{4/3}(bipy)_{1/2}(dabco)_{1/2}]$, henceforth referred to as MUF-32 (MUF = Massey University Framework). This MOF can be produced in the form of both a microcrystalline powder (MUF-32mc), and, if benzoic acid is added as a modulator to the reaction mixture, as high-quality single crystals (MUF-32sc). X-ray crystallography on MUF-32sc reveals that all three organic components are incorporated into unique positions in the lattice to produce a well-ordered MOF. Each ntb ligand coordinates to three dinuclear zinc(II) paddlewheels via its carboxyl groups to generate the underlying **pto** sublattice (Figure 1a and purple net in Figure 3b). The paddlewheels

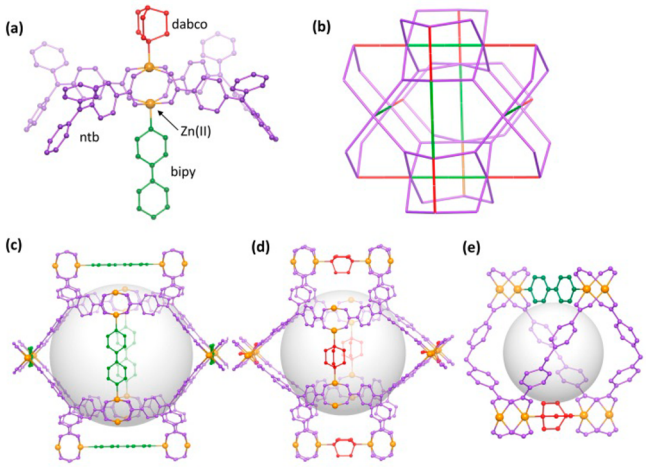

Figure 3. (a) The six-connected dinuclear zinc(II) SBU of MUF-32, highlighting the coordination of three different ligands. (b) The network structure of MUF-32 with the **pto** sublattice shown in purple. (c) The larger dodecahedral cavities of MUF-32 that are bounded by the bipy ligands. (d) The smaller dodecahedral cavities of MUF-32 that are bounded by the dabco ligands. (e) The tetrahedral cavities of MUF-32.

additionally coordinate to the nitrogen donor atoms of one bipy and one dabco ligand in their axial sites (Figure 3a). These linear ligands link the metal clusters to generate a network with **ith-d** topology. Three different cavities exist in MUF-32: two dodecahedral cavities with interatomic diameters of 25.8 and 24.3 Å (Figures 3c-d) and a smaller tetrahedral cavity (Figure 3e). MUF-32 joins a small group of known quaternary frameworks and is the first to feature neutral N-donor ligands.

Due to the large number of components in the reaction mixture, a number of phases that are derived from just one or two ligands can compete with MUF-32 during synthesis (Figure 2). Known compounds built up from $Zn(NO_3)_2$, ntb, dabco, and/or bipy include $[Zn_4O(ntb)_2]$ (MOF-150),[33] $[Zn(bipy)](NO_3)_2$,[34] and a variety of discrete Zn(II)-dabco complexes.[35] In spite of the existence of these competing phases, we were able to prepare phase-pure MUF-32 by optimization of the synthesis conditions. Yields were maximized by maintaining a high ratio of glass surface area to solvent volume in the reaction vessel. Bulk phase purity was established by ^{1}H NMR spectroscopy on dissolved samples (Figure S1), which confirms that the ligands are present in the expected ratios, and a match between the PXRD pattern of a bulk sample with the pattern calculated from the single-crystal structure (Figure S8). PXRD patterns recorded after exposure of MUF-32 to the atmosphere indicate that it has good stability under these conditions (Figure S8).

Following activation by solvent exchange with CH_2Cl_2, the permanent porosity of MUF-32 was established by gas adsorption. Its N_2 adsorption isotherm measured at 77 K displays a steep rise in the low pressure region followed by a plateau beyond $P/P_o \sim 0.08$ (Figures S9 and S11). This is consistent with the microporosity expected on the basis of its single-crystal structure. An apparent BET surface area of 2810 m^2/g can be calculated from the isotherm for MUF-32mc and 3260 m^2/g for MUF-32sc. The capacity of both forms of MUF-32 to adsorb CO_2, CH_4, and N_2 at 273 and 298 K was also assessed (Figures S10 and S12). Linear isotherms are observed in all cases. Relative uptake capacities follow the expected trend $CO_2 > CH_4 > N_2$ and are higher for MUF-32sc as compared to MUF-32mc owing to the higher accessible pore volume of the former (as evidenced by the N_2 uptake at 77 K).

Synthesis of MUF-21 and MUF-22. We subsequently sought to deliberately synthesize ternary MOFs from combinations of (i) ntb and bipy and (ii) ntb and dabco. This expands this family of multicomponent MOFs and enables confirmation (by PXRD) that these phases do not contaminate MUF-32.

Using synthetic conditions similar to those employed for MUF-32, the combination of zinc(II), H_3ntb, and bipy produces the ternary framework $[Zn_3(ntb)_2(bipy)_{3/2}(DMF)]$ (MUF-21). Using a linker set comprising H_3ntb and dabco, we observed formation of the ternary framework $[Zn_3(ntb)_2(dabco)]$ (MUF-22). MUF-21 and MUF-22 were characterized by single-crystal X-ray diffraction, thermogravimetric analysis (TGA), and gas adsorption isotherms. In MUF-21, three crystallographically independent zinc(II) SBUs − a paddlewheel and two mononuclear nodes − link the ntb and bipy linkers into a 3D network (Figure S5). This network

DOI: 10.1021/acs.chemmater.5b04306
Chem. Mater. 2016, 28, 368−375

comprises 2D sheets that are formed by the fusion of tubes that run along the crystallographic *b* direction. Adjacent sheets are interpenetrated. MUF-22 features an uncommon[36,37] type of eight-connected trinuclear zinc(II) SBU that links the ntb and dabco ligands into a 3D network (Figure S6). Channels with a cross-section of ~22 × 27 Å (interatomic distances) propagate along the *c* axis.[38]

N_2 adsorption isotherms measured at 77 K established the porosity of MUF-21 and MUF-22 following activation (Figures S13 and S14). For MUF-21, a steep rise in N_2 uptake up to $P/P_o \sim 0.01$ is followed by a near-plateau region between $P/P_o \sim 0.01-0.1$. This is consistent with the microporosity anticipated from the X-ray crystal structure. An upward inflection of the isotherm beyond $P/P_o = 0.02$ and hysteresis in the desorption curve in this region are consistent with a gradual gate-opening process. From a structural viewpoint, this is likely to be associated with movement of the interpenetrated sublattices relative to one another.[39,40] The Type I profile of the isotherm recorded for MUF-22, with a slight inflection at $P/P_o \sim 0.05$, is in keeping with the mesoporous nature of this framework. Its apparent BET surface area is 1810 m^2/g.

Defect Engineering in MUF-32. Several observations during the synthesis and handling of MUF-32 indicated that it was indeed amenable to high levels of bipy and dabco vacancy defects: (i) when adjusting the feed ratio of the three linkers to optimize the synthetic route to MUF-32 we noticed that frameworks with substoichiometric quantities of bipy were frequently produced; (ii) when pristine MUF-32 was washed with DMF some of the bipy dissociated from the framework into solution; (iii) TGA traces exhibited gradual weight loss at moderate temperatures, which could be traced to the expulsion of dabco from the framework.

We conducted a systematic investigation on the deliberate engineering of defects in MUF-32 (Figure 4). Both vacancy defects, specifically the absence of bipy or dabco ligands, and substitution defects, bipy or dabco being partially replaced by another ligand, are possible. As summarized in Table 2, defects were introduced to MUF-32 by three different routes. The deliganded frameworks are formulated as $[Zn_2(ntb)_{4/3}(bipy)_x(dabco)_y]$, where *x* and *y* deviate from the value of 1/2 observed in pristine MUF-32. Defects were quantified by ^{1}H NMR spectroscopy on digested frameworks on the assumption that, for reasons of charge balance, the ntb ligand sites are always fully occupied, and only the bipy and dabco ligands assume substoichiometric ratios.

Route 1: Introduction of Defects by de Novo Synthesis. MUF-32A-D (microcrystalline) and MUF-32G-J (single crystalline) with substoichiometric levels of bipy were directly synthesized by systematically reducing the amount of bipy in the synthesis mixture. Although SCXRD on MUF-32G-J was not possible due to the presence of multiple crystal domains (Figure S19), PXRD indicated that the overall architecture of MUF-32 was retained in all cases (Figures S18 and S23). The amount of bipy ligand incorporated into these materials was determined by ^{1}H NMR spectroscopy on digested samples. The creation of bipy absence defects correlates with an uptick in the amount of incorporated dabco linker, particularly for the single-crystalline materials (Table 2). In all cases, the total quantity of bipy and dabco per paddlewheel ($x + y$) does not exceed unity, which suggests that the dabco occupies some of the bipy sites in the lattice. Since major variations are not seen in the PXRD patterns of these materials, it is unlikely that the dabco ligand bridges two paddlewheels, since this would

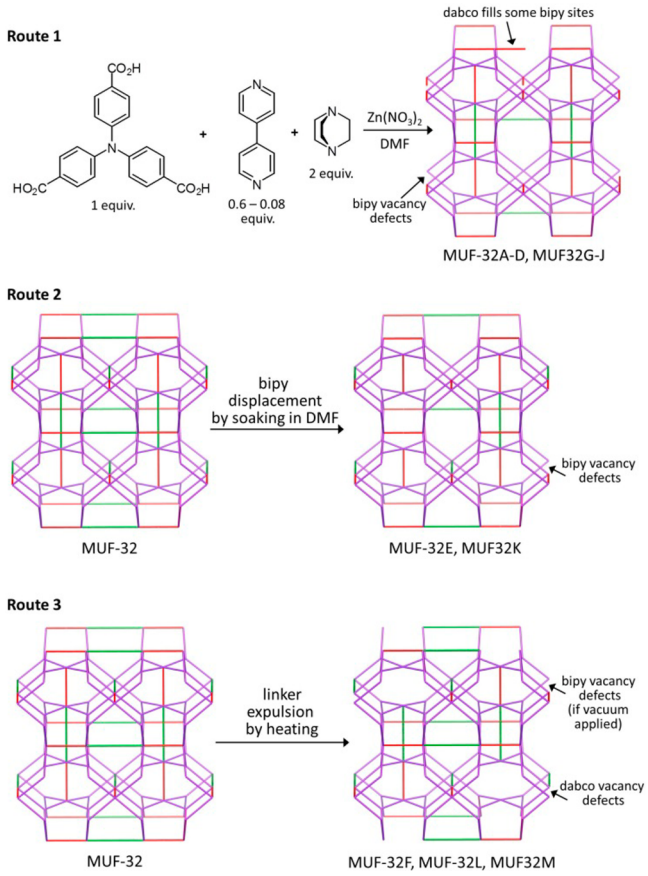

Figure 4. Three routes that were developed to create defects in MUF-32. The network structures of the MOFs are presented. Purple = ntb; green = bipy, red = dabco.

necessitate a significant structural reorganization, but rather that it coordinates to the framework by just one of its nitrogen donors (Figure S7). It is likely that solvent molecules, e.g. H_2O, DMF, fill the remaining coordination site on the paddlewheel cluster vacated by the bipy ligand.

Route 2: Postsynthetic Introduction of Defects by Soaking in DMF. Bipy is expelled from MUF-32mc and MUF-32sc simply by soaking in fresh DMF. When this method was employed for preparative purposes, the numerical superscript at the end of the sample code indicates the soaking period in minutes (Table 2). The release of bipy was confirmed by ^{1}H NMR spectroscopy of DMF-d_7 solvent in contact with solid samples of these materials (Figures S17, S24, and S25). Replacing DMF by CH_3NO_2 or CH_2Cl_2 in the soaking experiments led to no loss of the bipy ligand, which suggests that the ability of DMF to coordinate to the coordination site made vacant on the zinc SBU is important. The exchange of MOF ligands by solvent molecules has precedence in the literature.[41,42] Interestingly, many known examples involve the displacement of dabco linkers, rather than bipy as seen here. We posit that in this case bipy is expelled in preference to dabco owing to its weaker basicity. Steric effects may play a role, as well as entropic effects since bipy gains torsional degrees of freedom that dabco does not upon release into solvent.

Due to its smaller particle size, defect creation is much more rapid in MUF-32mc than in MUF-32sc; however, in both cases the amount of bipy ligands released from the lattice, as quantified by ^{1}H NMR spectroscopy on digested samples,

DOI: 10.1021/acs.chemmater.5b04306
Chem. Mater. 2016, 28, 368–375

Table 2. Summary of MUF-32 Materials with Vacancy Defects, Which Are Formulated as $[Zn_2(ntb)_{4/3}(bipy)_x(dabco)_y]$

	form[a]	route[b]	x[c]	y
Defect Creation				
MUF-32mc	**MC**	**pristine**	**0.50**	**0.50**
MUF-32A	MC	1	0.40	0.50
MUF-32B	MC	1	0.33	0.54
MUF-32C	MC	1	0.20	0.62
MUF-32D	MC	1	0.10	0.68
MUF-32E^3	MC	2	0.40	0.50
MUF-32E^{10}	MC	2	0.39	0.50
MUF-32E^{30}	MC	2	0.39	0.50
MUF-32F	MC	3[d]	0.47	0.26
MUF-32sc	**SC**	**pristine**	**0.50**	**0.50**
MUF-32G	SC	1	0.35	0.62
MUF-32H	SC	1	0.27	0.70
MUF-32I	SC	1	0.20	0.76
MUF-32J	SC	1	0.14	0.78
MUF-32K^{10}	SC	2	0.48	0.50
MUF-32K^{30}	SC	2	0.47	0.50
MUF-32K^{180}	SC	2	0.44	0.50
MUF-32K^{1440}	SC	2	0.40	0.50
MUF-32L	SC	3[d]	0.49	0.42
MUF-32M	SC	3[e]	0.37	0.32
Defect Healing				
MUF-32Bh	MC	4	0.44	0.53
MUF-32Dh	MC	4	0.21	0.68
MUF-32E^{3}h	MC	4	0.51	0.51
MUF-32Gh	SC	4	0.42	0.56
MUF-32Ih	SC	4	0.23	0.74
MUF-32K^{1440}h[f]	SC	4	0.50	0.50

[a]MC = microcrystalline powder, SC = large single crystals. [b]Route 1 = direct synthesis; Route 2 = washing with DMF, the superscripts on the sample codes indicate the lengths of time, in minutes, the sample was exposed to DMF; Route 3 = direct heating of solid sample; Route 4 = defect healing by soaking in a solution of bipy in CH_2Cl_2. [c]The stoichiometry of bipy and dabco was determined by ^{1}H NMR spectroscopy using the ntb peak integrals as a reference. [d]Heated to 150 °C in a TGA instrument. [e]Heated to 150 °C in a vacuum oven for 3 h. [f]By X-ray diffraction on a single crystal, x = 0.474(6).

plateaus at ∼20% (Figures S16 and S22). The overall network of MUF-32 is sustained upon displacement of the bipy linkers, as evidenced by PXRD patterns (Figures S18 and S23).

Route 3: Postsynthetic Introduction of Defects by Heating. The third route to generating defects in MUF-32 is heating to moderate temperatures. Deliganded MUF-32 frameworks, MUF-32F from MUF-32mc and MUF-32L from MUF-32sc, which are deficient in dabco are produced by this method (Table 2). The loss of dabco by heating is consistent with it being the most volatile of the framework components. Chun et al. have previously reported on the thermal expulsion of dabco from a MOF.[43]

The release of the dabco ligands could be monitored by TGA experiments where samples were heated to 150 °C and held at that temperature for 3 h (Figure S20). Since TGA cannot be used as a quantitative tool due to the unavoidable presence of volatile guest molecules that also contribute to the observed weight loss, we employed ^{1}H NMR spectroscopy on digested samples to assess the extent of dabco vacancy formation (Figures S15 and S21). Owing to its larger particle size, MUF-32sc releases dabco much less readily than MUF-32mc: only 16% of the dabco ligands are absent from MUF-32L, whereas ∼50% of the dabco linkers are expelled in producing MUF-32F. If the sample is placed in a vacuum chamber during heating, the reduced pressure results in significant loss of both the dabco and bipy ligands (MUF-32M). In all cases, PXRD clearly indicates that the overall structure of the parent MUF-32 framework is maintained following thermal defect generation (Figures S18 and S23).

Gas Adsorption Properties of Defect MUF-32 Materials. To assess the textural characteristics of deliganded MUF-32 materials, gas adsorption isotherms were measured. Crucially, MUF-32 maintains high levels of porosity — and thus its structural integrity — even when significant defects are introduced (Figure 5). This can be ascribed to its multicomponent nature: the underlying $[Zn_2(ntb)_{4/3}]$ sublattice provides a sound structural foundation that resists collapse when a significant fraction of the bipy and dabco ligands is absent.

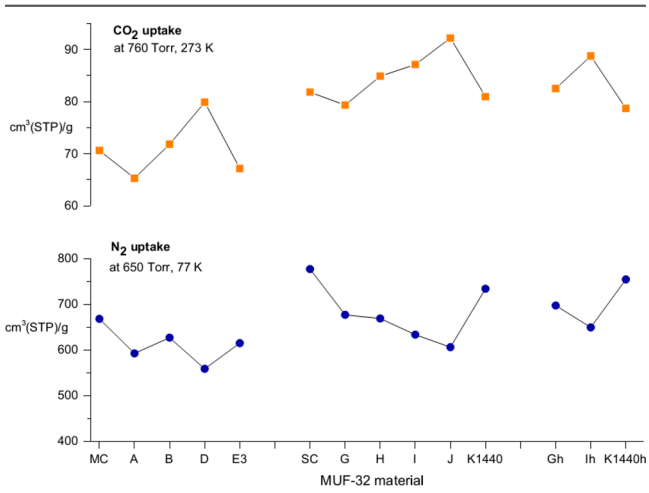

Figure 5. Plot showing N_2 (650 Torr, 77 K) and CO_2 (760 Torr, 273 K) capacities of MUF-32mc, MUF-32sc, and related defect and healed materials.

CO_2 adsorption isotherms measured on the microcrystalline materials at 273 K reveal several interesting trends (Figure 5). MUF-32A and MUF-32E^3, in which ∼20% of the bipy sites are vacant, adsorb fractionally less CO_2 than pristine MUF-32mc. On the other hand, despite taking up less N_2 at 77 K, MUF-32B and MUF-32D take up more CO_2. A greater number of bipy linkers are absent from these frameworks and some of these sites are occupied by dabco. Since in this situation the dabco coordinates in a monotopic fashion, this leaves one of its nitrogen atoms free to interact with guest molecules (Figure S7). Favorable electrostatic interactions between CO_2 molecules and the dabco nitrogen thus underlie the affinity of MUF-32B and MUF-32D for this gas.[44] The CO_2 capacity of MUF-32mc is increased by 15% in going to its deliganded analogue MUF-32D.

At 273 K, the CO_2 uptake capacities of the deliganded single-crystalline materials range from 79 to 92 cm^3(STP)/g (Figure 5). CO_2 uptake increases for the directly synthesized defect frameworks as progressively more of the bipy ligands are replaced by monotopic dabco ligands (MUF-32G-J). As outlined above, this can be ascribed to interactions between the CO_2 and the free dabco nitrogen atom. MUF-32H-J outperform MUF-32sc in terms of CO_2 adsorption despite

DOI: 10.1021/acs.chemmater.5b04306
Chem. Mater. 2016, 28, 368−375

having lower N_2uptake at 77 K. The postsynthetic removal of bipy ligands from MUF-32sc to give MUF-32K[1440] has little impact on the CO_2 uptake capacity.

Defect Healing. MUF-32E[3] and MUF-32K[1440] can be healed by soaking in a solution of bipy to regenerate pristine MUF-32 (Table 2). The success of the healing process was judged by ^{1}H NMR spectroscopy. For MUF-32K[1440], defect healing significantly improves its structural order, as evidenced by single-crystal X-ray diffraction patterns. Upon soaking MUF-32 single crystals in DMF for various periods to produce the MUF-32K^x materials, the diffraction quality is reduced. The diffraction spots become more diffuse and often split into multiple spots (Figure S28). This indicates that the long-range order in the lattice of MUF-32K is altered with respect to MUF-32sc and that multiple domains incommensurate with the parent structure likely develop upon defect formation. Upon healing the bipy vacancies in MUF-32K[1440] to generate MUF-32K[1440]h, sharp and single spots are restored to the diffraction pattern (Figure S28). Optical microscopy shows that the external form and transparency of the MUF-32 crystals are maintained through the defect production and healing steps. Gas adsorption measurements conducted on the healed single-crystalline materials MUF-32Gh, MUF-32Ih, and MUF-32K[1440]h indicate that high levels of porosity are maintained during the healing process (Figure 5).

For MUF-32Bh, MUF-32Dh, MUF-32Gh, and MUF-32Ih, healing of the defect frameworks produces materials other than pristine MUF-32. For example, MUF-32G has the formula $[Zn_2(ntb)_{4/3}(bipy)_{0.35}(dabco)_{0.62}]$, indicating that dabco occupies some of the bipy sites. Soaking MUF-32G in a solution of bipy in CH_2Cl_2 produces MUF-32Gh, $[Zn_2(ntb)_{4/3}(bipy)_{0.42}(dabco)_{0.56}]$. The reduction in the dabco content vis-a-vis MUF-32G indicates some of the dabco ligands residing in the bipy sites are displaced by incoming bipy ligands. However, the extent to which these "imposter" dabco ligands can be displaced has an upper limit, even after extensive exposure to a solution of bipy (Table 2). It is noteworthy that the sum of the bipy and dabco stoichiometries nears the maximum value of unity, implying that almost all bipy sites are occupied by either a bipy or a dabco linker.

Computational Analysis. To further understand the ability of MUF-32 to tolerate defects we performed quantum-chemistry calculations at the Density Functional Theory (DFT) level for eight crystalline structures of formula $[Zn_2(ntb)_{4/3}(bipy)_x(dabco)_y]$, with $0 \le x, y \le 1/2$. We focused on the relative energies of these materials and their mechanical stability. Ordered models with various compositions were generated from the MUF-32 crystallographic structure by removal of bipy or dabco ligands (Table S3). Energy minimization was then performed for each model, giving both a relaxed structure and its energy. The structures calculated in this way are in good agreement with the crystallographic coordinates (Figure S47). On the basis of the relaxed structures, second-order elastic constants were calculated and the elastic properties analyzed following a procedure established in earlier literature.[45,46]

The computational results underscore the utility of multicomponent MOFs creating materials with high levels of defects:

(i) The calculated unit cell volume and cell parameters of the defective frameworks were found to vary only slightly (±1.7%) from MUF-32 (Table 3), which shows that the creation of defect does not involve a substantial structural reorganization. This is consistent with the experimental PXRD patterns. One geometric parameter that does change between calculated structures of MUF-32 and $[Zn_2(ntb)_{4/3}]$ is the distance between the paddlewheels. In the latter it adopts a uniform value and does not alternate between short (dabco sites) and long (bipy sites) values as it does in MUF-32. The insertion of both bipy and dabco linkers to link the axial sites of the paddlewheel SBUs therefore does involve a local deformation; however, it results in minimal strain on the $[Zn_2(ntb)_{4/3}]$ sublattice.

Table 3. Structural and Mechanical Properties of Eight Frameworks with Formulas $[Zn_2(ntb)_{4/3}(bipy)_x(dabco)_y]$ as Calculated by Density Functional Theory[a]

(x, y)	MOF	ΔV (%)	φ	S	E	G
(1/2, 1/2)	MUF-32	0	0.45	3920	5.24	1.84
(1/3, 1/2)	defect	−0.47	0.46	3980		
(1/6, 1/2)	defect	−1.21	0.48	4040		
(0, 1/2)	defect	−1.74	0.50	4120	2.89	0.99
(1/2, 0)	defect	−0.24	0.47	4460		
(1/3, 0)	defect	0.13	0.50	4520		
(1/6, 0)	defect	0.66	0.52	4590		
(0, 0)	$[Zn_2(ntb)_{4/3}]$	1.68	0.55	4670	1.60	0.54

[a]Quantities listed: volume variation, (ΔV) with respect to MUF-32 (in percent), porosity φ, accessible surface area S (in cm^2/g), spatially averaged Young's (E), and shear (G) moduli, both in GPa.

(ii) Although not experimentally observed, $[Zn_2(ntb)_{4/3}]$ was found to be energetically feasible since it corresponds to a local energy minimum. The same holds for the structures with (x, y) = (1/2, 0) and (0, 1/2). Rather than compare absolute energies, which is fraught with difficulty for these kinds of materials, we calculated the binding energies of the bipy and dabco ligands to these structures. The binding energies to the $[Zn_2(ntb)_{4/3}]$ sublattice are 238 kJ/mol (bipy) and 329 kJ/mol (dabco) per ligand. The stronger binding of dabco is in agreement with experimental observations that this ligand is generally more difficult to remove from MUF-32 when generating vacancy defects by direct synthesis or ligand exchange (Routes 1 and 2).

We found that these binding energies do not depend strongly on the composition of the rest of the framework. For bipy, where compositions of x = 0, 1/6, 1/3, and 1/2 were tested, we observe that the binding energy has only a slight (and almost linear) dependency on the number of vacancies, varying between 233 and 242 kJ/mol. Likewise, the binding energy of dabco to $[Zn_2(ntb)_{4/3}(bipy)_{1/2}]$ is only marginally smaller (303 kJ/mol) than that to $[Zn_2(ntb)_{4/3}]$ (329 kJ/mol). Thus, from an energetic perspective, there is no barrier to creating $[Zn_2(ntb)_{4/3}(bipy)_x(dabco)_y]$ materials with any values of x and y between 0 and 1/2.

(iii) Geometric pore space analysis was performed on the relaxed structures. Porosity (φ) decreases monotonously with both x and y, ranging from φ = 0.45 (MUF-32) to φ = 0.55 ($[Zn_2(ntb)_{4/3}]$). The surface area S (in cm^2/g) is found to increase slightly upon ligand removal owing to the decrease in mass. It is interesting to note that the variation of S observed upon varying x is smaller than the variations in BET surfaces as extracted from N_2 adsorption experiments. There are thus additional aspects than pure geometric considerations that drive the adsorption in the deliganded MUF-32, such as the presence of guest molecules inside the pores or flexibility of the framework. Additional theoretical work on adsorption properties will be needed to settle this question.

DOI: 10.1021/acs.chemmater.5b04306
Chem. Mater. 2016, 28, 368−375

(iv) Bulk modulus, which quantifies the volumetric response to isotropic compression, is almost unaffected by ligand removal (Table S4), meaning that the global stiffness of all MUF-32 materials is mostly determined by the underlying $[Zn_2(ntb)_{4/3}]$ sublattice. However, large changes are seen in the Young's and shear moduli, i.e. responses to uniaxial compression and shearing. In particular, the spatially averaged shear modulus, equal to 1.84 GPa in pristine MUF-32, is decreased to 0.99 GPa upon total removal of bipy [to $Zn_2(ntb)_{4/3}(dabco)_{1/2}$] and further to 0.54 GPa in $[Zn_2(ntb)_{4/3}]$. The Young's moduli follow the same trend: the lower connectivity of the metal clusters in deliganded MOFs renders the substoichiometric lattices more susceptible to both shear forces and compression along the directions of missing linkers.

The small value of shear modulus in $[Zn_2(ntb)_{4/3}]$ reveals why compounds with high proportions of both bipy and dabco vacancies, including $[Zn_2(ntb)_{4/3}]$ itself, are not observed. Although energetically feasible, it is the *mechanical* properties of MUF-32 that set an upper limit on the extent to which it can sustain vacancy defects. This situation is similar to that of hypothetical ZIF frameworks which, although of relatively low formation enthalpy,[47] are not mechanically stable enough to be able to be synthesized.[48] This theoretical study is the first to demonstrate the relationship between ligand vacancies and mechanical properties in MOFs and parallels some recent work by Cliffe et al. showing the dependence of thermal properties on the concentration of defects in UiO-66(Hf).[49]

CONCLUSION AND OUTLOOK

We have established a new strategy for deliberately introducing vacancy defects in MOFs. This strategy relies on coassembling both load-bearing and decorative components into the same framework. An underlying three-dimensional sublattice is maintained by the metal cluster and one of the linkers. Since the two other linkers are neutral and not essential for the structural integrity of the network, the network can be sustained when they are present at substoichiometric levels. Defects can be introduced in multiple ways, involving both *de novo* synthesis and postsynthetic modification, and defect levels can be used to tune the adsorption properties. In addition, we have shown how defect healing can restore the pristine parent MOF or produce a range of new materials. More broadly, our strategy can be viewed as an example of the recently introduced principle of 'using weakness as a synthetic tool,'[50] and contributes a new angle to the current surge of interest in MOFs with defects.[17] Taking advantage of multicomponent ligand sets to rationally engineer "defectogenic" frameworks promises to be a widely applicable methodology for fabricating materials with novel structural features and properties.

ASSOCIATED CONTENT

Supporting Information

The Supporting Information is available free of charge on the ACS Publications website at DOI: 10.1021/acs.chemmater.5b04306.

Crystallographic information (CIF) file (CIF)

Crystallographic information (CIF) file (CIF)

Additional characterization data (TXT)

Experimental and computational details (PDF)

AUTHOR INFORMATION

Corresponding Author

*E-mail: s.telfer@massey.ac.nz.

Notes

The authors declare no competing financial interest.

ACKNOWLEDGMENTS

We thank Dr. Hui Yang for valuable experimental assistance and advice. S.G.T. is grateful to the RSNZ Marsden Fund for supporting this research, and F.T. and F.X.C. acknowledge access to HPC resources provided by GENCI (grant i2015087069).

REFERENCES

(1) Burrows, A. D. Mixed-Component Metal-Organic Frameworks (MC-MOFs): Enhancing Functionality through Solid Solution Formation and Surface Modifications. *CrystEngComm* **2011**, *13*, 3623−3642.

(2) Bunck, D. N.; Dichtel, W. R. Mixed Linker Strategies for Organic Framework Functionalization. *Chem. - Eur. J.* **2013**, *19*, 818−827.

(3) Deng, H.; Doonan, C. J.; Furukawa, H.; Ferreira, R. B.; Towne, J.; Knobler, C. B.; Wang, B.; Yaghi, O. M. Multiple Functional Groups of Varying Ratios in Metal-Organic Frameworks. *Science* **2010**, *327*, 846−850.

(4) Park, T.-H.; Koh, K.; Wong-Foy, A. G.; Matzger, A. J. Nonlinear Properties in Coordination Copolymers Derived from Randomly Mixed Ligands. *Cryst. Growth Des.* **2011**, *11*, 2059−2063.

(5) Liu, L.; Konstas, K.; Hill, M. R.; Telfer, S. G. Programmed Pore Architectures in Modular Quaternary Metal−Organic Frameworks. *J. Am. Chem. Soc.* **2013**, *135*, 17731−17734.

(6) Liu, L.; Telfer, S. G. Systematic Ligand Modulation Enhances the Moisture Stability and Gas Sorption Characteristics of Quaternary Metal-Organic Frameworks. *J. Am. Chem. Soc.* **2015**, *137*, 3901−3909.

(7) Dutta, A.; Wong-Foy, A. G.; Matzger, A. J. Coordination Copolymerization of Three Carboxylate Linkers into a Pillared Layer Framework. *Chem. Sci.* **2014**, *5*, 3729−3734.

(8) Koh, K.; Oosterhout, J. D. V.; Roy, S.; Wong-Foy, A. G.; Matzger, A. J. Exceptional surface area from coordination copolymers derived from two linear linkers of differing lengths. *Chem. Sci.* **2012**, *3*, 2429−2432.

(9) Koh, K.; Wong-Foy, A. G.; Matzger, A. J. Coordination Copolymerization Mediated by $Zn_4O(CO_2R)_6$ Metal Clusters: A Balancing Act between Statistics and Geometry. *J. Am. Chem. Soc.* **2010**, *132*, 15005−15010.

(10) Grunker, R.; Bon, V.; Muller, P.; Stoeck, U.; Krause, S.; Mueller, U.; Senkovska, I.; Kaskel, S. A New Metal-Organic Framework with Ultra-High Surface Area. *Chem. Commun.* **2014**, *50*, 3450−3452.

(11) Helten, S.; Sahoo, B.; Bon, V.; Senkovska, I.; Kaskel, S.; Glorius, F. Copolymerisation at Work: The First Example of a Highly Porous MOF Comprising a Triarylborane-Based Linker. *CrystEngComm* **2015**, *17*, 307−312.

(12) Klein, N.; Senkovska, I.; Baburin, I. A.; Grünker, R.; Stoeck, U.; Schlichtenmayer, M.; Streppel, B.; Mueller, U.; Leoni, S.; Hirscher, M.; Kaskel, S. Route to a Family of Robust, Non-Interpenetrated Metal−Organic Frameworks with Pto-Like Topology. *Chem. - Eur. J.* **2011**, *17*, 13007−13016.

(13) Müller, P.; Wisser, F. M.; Bon, V.; Grünker, R.; Senkovska, I.; Kaskel, S. Postsynthetic Paddle-Wheel Cross-Linking and Functionalization of 1,3-Phenylenebis(Azanetriyl)Tetrabenzoate-Based MOFs. *Chem. Mater.* **2015**, *27*, 2460−2467.

(14) Furukawa, H.; Ko, N.; Go, Y. B.; Aratani, N.; Choi, S. B.; Choi, E.; Yazaydin, A. Ö.; Snurr, R. Q.; O'Keeffe, M.; Kim, J.; Yaghi, O. M. Ultrahigh Porosity in Metal-Organic Frameworks. *Science* **2010**, *329*, 424−428.

(15) Dutta, A.; Ma, J.; Wong-Foy, A. G.; Matzger, A. J. A Non-Regular Layer Arrangement of a Pillared-Layer Coordination Polymer:

DOI: 10.1021/acs.chemmater.5b04306
Chem. Mater. 2016, 28, 368−375

Avoiding Interpenetration Via Symmetry Breaking at Nodes. *Chem. Commun.* **2015**, *51*, 13611−13614.
(16) Koh, K.; Wong-Foy, A. G.; Matzger, A. J. A Crystalline Mesoporous Coordination Copolymer with High Microporosity. *Angew. Chem., Int. Ed.* **2008**, *47*, 677−680.
(17) Fang, Z.; Bueken, B.; De Vos, D. E.; Fischer, R. A. Defect-Engineered Metal−Organic Frameworks. *Angew. Chem., Int. Ed.* **2015**, *54*, 7234−7254.
(18) Tu, B.; Pang, Q.; Wu, D.; Song, Y.; Weng, L.; Li, Q. Ordered Vacancies and Their Chemistry in Metal-Organic Frameworks. *J. Am. Chem. Soc.* **2014**, *136*, 14465−14471.
(19) Vermoortele, F.; Bueken, B.; Le Bars, G.; Van de Voorde, B.; Vandichel, M.; Houthoofd, K.; Vimont, A.; Daturi, M.; Waroquier, M.; Van Speybroeck, V.; Kirschhock, C.; De Vos, D. E. Synthesis Modulation as a Tool to Increase the Catalytic Activity of Metal-Organic Frameworks: The Unique Case of UiO-66(Zr). *J. Am. Chem. Soc.* **2013**, *135*, 11465−11468.
(20) Cliffe, M. J.; Wan, W.; Zou, X.; Chater, P. A.; Kleppe, A. K.; Tucker, M. G.; Wilhelm, H.; Funnell, N. P.; Coudert, F. X.; Goodwin, A. L. Correlated Defect Nanoregions in a Metal−Organic Framework. *Nat. Commun.* **2014**, *5*, 4176.
(21) Katzenmeyer, A. M.; Canivet, J.; Holland, G.; Farrusseng, D.; Centrone, A. Assessing Chemical Heterogeneity at the Nanoscale in Mixed-Ligand Metal-Organic Frameworks with the PTIR Technique. *Angew. Chem., Int. Ed.* **2014**, *53*, 2852−2856.
(22) Han, D.; Jiang, F.-L.; Wu, M.-Y.; Chen, L.; Chen, Q.-H.; Hong, M.-C. A Non-Interpenetrated Porous Metal-Organic Framework with High Gas-Uptake Capacity. *Chem. Commun.* **2011**, *47*, 9861−9863.
(23) Klein, N.; Senkovska, I.; Baburin, I. A.; Grünker, R.; Stoeck, U.; Schlichtenmayer, M.; Streppel, B.; Mueller, U.; Leoni, S.; Hirscher, M.; Kaskel, S. Route to a Family of Robust, Non-Interpenetrated Metal−Organic Frameworks with pto-Like Topology. *Chem. - Eur. J.* **2011**, *17*, 13007−13016.
(24) Ko, N.; Noh, K.; Sung, S.; Park, H. J.; Park, S. Y.; Kim, J. Connection of Zinc Paddle-Wheels in a pto-Type Metal-Organic Framework with 2-Methylimidazolate and Subsequent Incorporation of Charged Organic Guests. *Chem. Commun.* **2014**, *50*, 6785−6788.
(25) O'Keeffe, M.; Peskov, M. A.; Ramsden, S. J.; Yaghi, O. M. The Reticular Chemistry Structure Resource (RCSR) Database of, and Symbols for, Crystal Nets. *Acc. Chem. Res.* **2008**, *41*, 1782−1789.
(26) Li, M.; Li, D.; O'Keeffe, M.; Yaghi, O. M. Topological Analysis of Metal−Organic Frameworks with Polytopic Linkers and/or Multiple Building Units and the Minimal Transitivity Principle. *Chem. Rev.* **2014**, *114*, 1343−1370.
(27) He, Y.; Guo, Z.; Xiang, S.; Zhang, Z.; Zhou, W.; Fronczek, F. R.; Parkin, S.; Hyde, S. T.; O'Keeffe, M.; Chen, B. Metastable Interwoven Mesoporous Metal−Organic Frameworks. *Inorg. Chem.* **2013**, *52*, 11580−11584.
(28) Furukawa, H.; Go, Y. B.; Ko, N.; Park, Y. K.; Uribe-Romo, F. J.; Kim, J.; O'Keeffe, M.; Yaghi, O. M. Isoreticular Expansion of Metal−Organic Frameworks with Triangular and Square Building Units and the Lowest Calculated Density for Porous Crystals. *Inorg. Chem.* **2011**, *50*, 9147−9152.
(29) Zhu, N.; Lennox, M. J.; Duren, T.; Schmitt, W. Polymorphism of Metal-Organic Frameworks: Direct Comparison of Structures and Theoretical N_2-Uptake of Topological pto- and tbo-Isomers. *Chem. Commun.* **2014**, *50*, 4207−4210.
(30) Johnson, J. A.; Chen, S.; Reeson, T. C.; Chen, Y.-S.; Zeng, X. C.; Zhang, J. Direct X-Ray Observation of Trapped Co_2 in a Predesigned Porphyrinic Metal−Organic Framework. *Chem. - Eur. J.* **2014**, *20*, 7632−7637.
(31) Zhao, T.; Jing, X.; Wang, J.; Wang, D.; Li, G.; Huo, Q.; Liu, Y. Assembly of Two 3d Porous Metal−Organic Frameworks Based on 1,2,3-Triazole-4,5-Dicarboxylate Exhibiting Novel Coordination Modes. *Cryst. Growth Des.* **2012**, *12*, 5456−5461.
(32) Klein, N.; Senkovska, I.; Gedrich, K.; Stoeck, U.; Henschel, A.; Mueller, U.; Kaskel, S. A Mesoporous Metal−Organic Framework. *Angew. Chem., Int. Ed.* **2009**, *48*, 9954−9957.
(33) Chae, H. K.; Kim, J.; Friedrichs, O. D.; O'Keeffe, M.; Yaghi, O. M. Design of Frameworks with Mixed Triangular and Octahedral Building Blocks Exemplified by the Structure of $[Zn_4O(tca)_2]$ Having the Pyrite Topology. *Angew. Chem., Int. Ed.* **2003**, *42*, 3907−3909.
(34) Ahuja, I. S.; Singh, R.; Rai, C. P. Preparation and Characterization of Divalent Cobalt, Nickel, Zinc, Cadmium and Monovalent Silver Nitrate Complexes with 4.4′-Bipyridine. *J. Inorg. Nucl. Chem.* **1978**, *40*, 924−926.
(35) Petrusenko, S. R.; Sieler, J.; Kokozay, V. N. Direct Synthesis of Zinc and Nickel(II) Complexes with 1,4-Diazabicyclo[2.2.2]octane. *Z. Naturforsch., B: J. Chem. Sci.* **1997**, *52*, 331−336.
(36) Tranchemontagne, D. J.; Mendoza-Cortes, J. L.; O'Keeffe, M.; Yaghi, O. M. Secondary Building Units, Nets and Bonding in the Chemistry of Metal-Organic Frameworks. *Chem. Soc. Rev.* **2009**, *38*, 1257−1283.
(37) Garibay, S. J.; Stork, J. R.; Wang, Z.; Cohen, S. M.; Telfer, S. G. Enantiopure Vs. Racemic Metalloligands: Impact on Metal−Organic Framework Structure and Synthesis. *Chem. Commun.* **2007**, 4881−4883.
(38) While this work was in progress the structure of MUF-21 was reported elsewhere: Zhao, M.; Su, J.; Zhang, J.; Wu, J.-Y.; Tian, Y.-P. A Zinc(II) Metal-Organic Framework with a Novel Topology Formed from 4,4',4''-Nitrilotribenzoate and 4,4'-Bipyridine Ligands. *Acta Crystallogr., Sect. C: Struct. Chem.* **2015**, *71*, 799−803.
(39) Furukawa, S.; Sakata, Y.; Kitagawa, S. Control over Flexibility of Entangled Porous Coordination Frameworks by Molecular and Mesoscopic Chemistries. *Chem. Lett.* **2013**, *42*, 570−576.
(40) Horike, S.; Shimomura, S.; Kitagawa, S. Soft Porous Crystals. *Nat. Chem.* **2009**, *1*, 695−704.
(41) Tan, K.; Nijem, N.; Canepa, P.; Gong, Q.; Li, J.; Thonhauser, T.; Chabal, Y. J. Stability and Hydrolyzation of Metal Organic Frameworks with Paddle-Wheel Sbus Upon Hydration. *Chem. Mater.* **2012**, *24*, 3153−3167.
(42) Chen, Z.; Xiang, S.; Zhao, D.; Chen, B. Reversible Two-Dimensional−Three Dimensional Framework Transformation within a Prototype Metal−Organic Framework. *Cryst. Growth Des.* **2009**, *9*, 5293−5296.
(43) Chun, H.; Bak, W.; Hong, K.; Moon, D. A Simple and Rational Approach for Binodal Metal−Organic Frameworks with Tetrahedral Nodes and Unexpected Multimodal Porosities from Nonstoichiometric Defects. *Cryst. Growth Des.* **2014**, *14*, 1998−2002.
(44) Sumida, K.; Rogow, D. L.; Mason, J. A.; McDonald, T. M.; Bloch, E. D.; Herm, Z. R.; Bae, T.-H.; Long, J. R. Carbon Dioxide Capture in Metal−Organic Frameworks. *Chem. Rev.* **2012**, *112*, 724−781.
(45) Ortiz, A. U.; Boutin, A.; Fuchs, A. H.; Coudert, F.-X. Anisotropic Elastic Properties of Flexible Metal-Organic Frameworks: How Soft Are Soft Porous Crystals? *Phys. Rev. Lett.* **2012**, *109*, 195502.
(46) Ortiz, A. U.; Boutin, A.; Fuchs, A. H.; Coudert, F.-X. Metal−Organic Frameworks with Wine-Rack Motif: What Determines Their Flexibility and Elastic Properties? *J. Chem. Phys.* **2013**, *138*, 174703.
(47) Lewis, D. W.; Ruiz-Salvador, A. R.; Gomez, A.; Rodriguez-Albelo, L. M.; Coudert, F.-X.; Slater, B.; Cheetham, A. K.; Mellot-Draznieks, C. Zeolitic Imidazole Frameworks: Structural and Energetics Trends Compared with Their Zeolite Analogues. *CrystEngComm* **2009**, *11*, 2272−2276.
(48) Bouëssel du Bourg, L.; Ortiz, A. U.; Boutin, A.; Coudert, F.-X. Thermal and Mechanical Stability of Zeolitic Imidazolate Frameworks Polymorphs. *APL Mater.* **2014**, *2*, 124110.
(49) Cliffe, M. J.; Hill, J. A.; Murray, C. A.; Coudert, F.-X.; Goodwin, A. L. Defect-Dependent Colossal Negative Thermal Expansion in UiO-66(Hf) Metal-Organic Framework. *Phys. Chem. Chem. Phys.* **2015**, *17*, 11586−11592.
(50) Morris, R. E.; Cejka, J. Exploiting Chemically Selective Weakness in Solids as a Route to New Porous Materials. *Nat. Chem.* **2015**, *7*, 381−388.

DOI: 10.1021/acs.chemmater.5b04306
Chem. Mater. 2016, 28, 368−375